

## Bioactive DNA-Peptide Nanotubes Enhance the Differentiation of Neural Stem Cells Into Neurons

Nicholas Stephanopoulos,<sup>†</sup> Ronit Freeman,<sup>†</sup> Hilary A. North,<sup>‡</sup> Shantanu Sur,<sup>†</sup> Su Ji Jeong,<sup>‡</sup> Faifan Tantakitti,<sup>†,§</sup> John A. Kessler,<sup>‡</sup> and Samuel I. Stupp\*,<sup>†,§,||,⊥</sup>

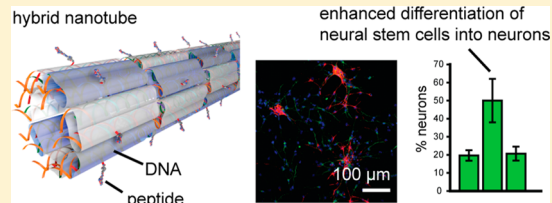
<sup>†</sup>Simpson Querrey Institute for BioNanotechnology, Feinberg School of Medicine and <sup>‡</sup>Department of Neurology, Northwestern University, Chicago, Illinois 60611, United States

<sup>§</sup>Department of Materials Science and Engineering and <sup>||</sup>Department of Chemistry, Northwestern University, Evanston, Illinois 60208, United States

<sup>⊥</sup>Department of Medicine, Northwestern University, Chicago, Illinois 60611, United States

### Supporting Information

**ABSTRACT:** We report the construction of DNA nanotubes covalently functionalized with the cell adhesion peptide RGDS as a bioactive substrate for neural stem cell differentiation. Alteration of the Watson–Crick base pairing program that builds the nanostructures allowed us to probe independently the effect of nanotube architecture and peptide bioactivity on stem cell differentiation. We found that both factors instruct synergistically the preferential differentiation of the cells into neurons rather than astrocytes.



**KEYWORDS:** *Self-assembly, biomaterials, DNA nanotechnology, extracellular matrix, DNA-peptide, neural stem cells*

Supramolecular nanostructures with biological information are highly promising for learning structure–function relationships in biology and for the development of materials for medicine. One example is the use of self-assembled nanostructures that mimic the extracellular matrix (ECM) and display biological signals to instruct cell behavior. In this context, there is a need for strategies to create nanostructures that are structurally programmable and easily modified with signaling components. DNA has emerged as one of the most promising building blocks for nanoscale assemblies due to the highly predictable nature of Watson–Crick base pairing, enabling the formation of nanostructures with immense shape diversity.<sup>1,2</sup> These advantages allow for unprecedented control of nanoscale architecture through design of appropriate DNA sequences, including one-,<sup>3–5</sup> two-,<sup>6</sup> and three-dimensional structures, and highly complex objects such as those exemplified by DNA origami.<sup>8–10</sup> The defined molecular dimensions of DNA enable the site-specific arrangement of different components such as nanoparticles<sup>11</sup> and proteins<sup>12</sup> with nanometer precision. In the context of biomedicine, a number of reports have demonstrated the potential of DNA for disease diagnosis and treatment, especially in the areas of biosensing, vaccine development, and drug delivery.<sup>13–18</sup>

An area that has been only scarcely explored is the use of DNA nanostructures as artificial scaffolds to control cell behavior. One previous notable example is the use of DNA ribbons coated on a glass substrate and subsequently conjugated to domains of the extracellular matrix protein, fibronectin, to promote cell adhesion and control cell morphology.<sup>19</sup> Several other reports describe the use of

reversible DNA hydrogels to encapsulate and release cells.<sup>20,21</sup> However, the integration of DNA nanotechnology with bioactive peptides in systems that could impact regenerative medicine has been a major gap in the field.

Nanostructures utilizing peptides as building blocks<sup>22</sup> have been extensively studied in the context of regenerative medicine. In particular, peptide amphiphiles (PAs), a class of molecules in which a peptide sequence is conjugated to a hydrophobic segment,<sup>23</sup> are known to form high aspect ratio nanofibers that emulate components of the mammalian ECM and direct processes as complex as neural stem cell differentiation,<sup>24</sup> angiogenesis,<sup>25,26</sup> bone<sup>27,28</sup> and cartilage regeneration,<sup>29</sup> among others. Despite the many advantages of self-assembling peptide-based materials, several limitations remain. Because the peptide sequence contains both the self-assembling motif and the relevant biological epitope, the bioactive cues (especially those that differ in size or charge) can potentially influence the self-assembly process, making it difficult to predict the exact nanostructure that will be formed. In addition, it is challenging to present, through self-assembly, multiple epitopes with nanoscale spatial control. In this work, we report on the coassembly of DNA and peptide-DNA hybrid molecules to simultaneously define architecture and bioactivity. The coassemblies investigated formed nanotubes capable of guiding the differentiation of neural stem cells into neurons.

**Received:** October 23, 2014

**Revised:** December 17, 2014

**Published:** December 29, 2014

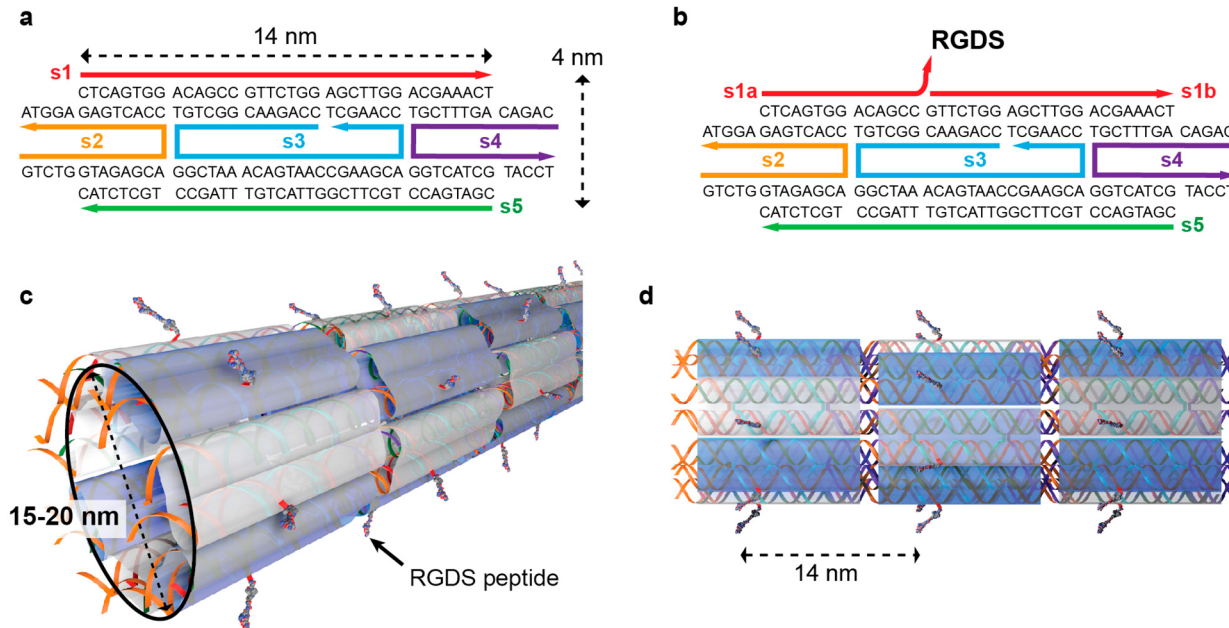


**Figure 1.** Design of the DNA nanotubes. (a) Five strands (labeled s1–5) self-assemble to form a double-crossover tile, approximately 14 nm in length and 4 nm in width. Arrows are drawn from the 5' to 3' ends of the DNA strand. (b) Breaking s1 into two strands (s1a and s1b) and modifying s1a with the peptide sequence RGDS allows for display of the epitope from the tube surface. The location of the break point was chosen based on previous reports to allow the peptide to extend outward from the tube surface. (c) Illustration of the assembled RGDS-modified nanotubes, demonstrating the relative arrangement of the tiles and the relative size of the peptide compared to the DNA. The tiles are identical but are shaded differently for contrast. Unmodified nanotubes are the same but without the peptide attached. (d) Side view of the RGDS-modified nanotubes.

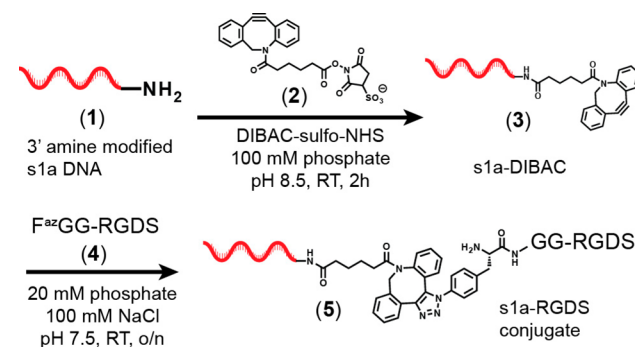
We chose a DNA design that resembles the high aspect ratio PA nanofibers, since these are well-known to be effective as ECM mimics for regenerative medicine. We therefore adapted for our system a DNA nanotube design, first reported by Rothmund et al.,<sup>3</sup> and further developed by others.<sup>30,31</sup> The starting design for the nanotubes, adapted from ref 31., is shown in Figure 1. It consists of five DNA strands (denoted s1–5) that self-assemble into a two-dimensional “tile” consisting of two parallel DNA helices (Figure 1a). The design contains two points where the strands cross over from one helix to the next in an antiparallel fashion, resulting in a “double-crossover” tile. The edges of the tile contain short single-stranded DNA segments that direct the assembly of the tile into a two-dimensional lattice; however, due to the design of the tile and helical properties of DNA,<sup>3</sup> this lattice curves and forms a closed nanotube structure (Figure 1c,d). These nanotubes generally consist of 7–10 tiles in circumference, corresponding to a diameter of 14–20 nm, and can reach many microns in length.

As originally designed, the nanotubes are composed exclusively of tightly packed double-helical DNA and do not possess any known biological epitopes for cell receptors. In order to endow them with biological activity and use them as substrates for cell attachment and differentiation, we split one of the strands (s1) comprising the tile into two fragments (s1a, s1b) at a location previously shown to extend outward from the tube.<sup>3,31</sup> We attached a bioactive peptide to the s1a strand (Figure 1b), resulting in nanotubes with one peptide per tile with a periodicity of 14 nm along the tile axis, and 4 nm around its circumference, as shown in Figure 1c,d. The peptide selected was the epitope RGDS derived from fibronectin because of its potent cell-binding activity (via integrin receptors, among others), and its widespread use in biomaterials for the

attachment, proliferation, and differentiation of various cell populations.<sup>32,33</sup>

The peptide was conjugated to the DNA strand using the Huisgen 1,3-dipolar cycloaddition reaction between a strained cyclooctyne and an azide, commonly referred to as “copper-free click” (Scheme 1).<sup>34,35</sup> This reaction is highly selective for the

#### Scheme 1. Synthesis of DNA-Peptide Conjugates



cyclooctyne and azide functional groups, proceeds quickly and efficiently in water at room temperature and neutral pH, and both the starting materials and products are stable to most storage or reaction conditions. We reacted the 3'-amine-modified s1a DNA 1 with dibenzocyclooctyne-sulfo-N-hydroxysuccinimidyl ester (DIBAC-sulfo-NHS, 2) to generate the s1a-DIBAC conjugate 3. After removal of excess 2, we exposed this DNA conjugate to azide-containing peptide F<sup>az</sup>GGRGDS 4 synthesized via solid-phase peptide synthesis, where F<sup>az</sup> denotes the unnatural amino acid 4-azido-L-phenylalanine (Supporting Information Figure S1). The resulting s1a-RGDS molecule 5 was isolated by reverse phase high-performance liquid chromatography (HPLC) and ob-

tained as a highly pure conjugate (see Supporting Information for detailed synthesis, purification, and characterization of the peptides and peptide-DNA conjugates).

We first examined whether incorporating the RGDS epitope (a system that we term **RGDS-NT**) would yield nanotubes with the same efficiency as the unmodified system (which we term **bare-NT**). We mixed the constituent strands (s1–5 for **bare-NT**, and s1a-RGDS, s1b, and s2–5 for **RGDS-NT**) at 25  $\mu\text{M}$  each and annealed the solution from 95 to 20 °C over 5 h. After annealing, we examined the resulting structures by cryogenic transmission electron microscopy (cryoTEM), a technique that most accurately represents the native assembly state of structures in solution. It should be noted that in **RGDS-NT**, only strands s1a-RGDS and s1b were added to the annealing mixture but no s1. Thus, all tubes formed must contain the peptide because the structures cannot form in the absence of any single strand. As seen in Figure 2a and

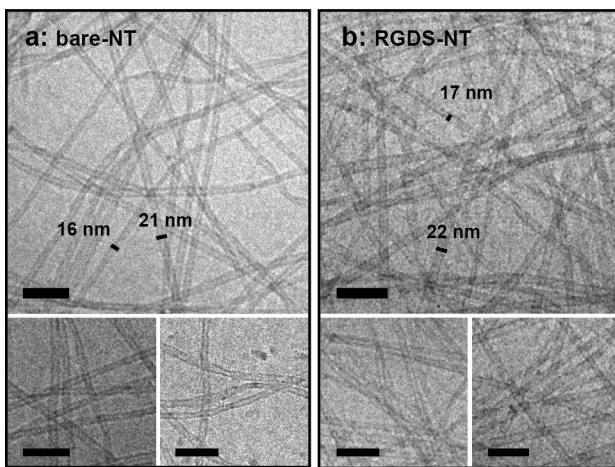


**Figure 2.** CryoTEM characterization of DNA nanotubes. Both the unmodified, bare DNA (a) and RGDS-modified (b) nanotube systems self-assemble into hollow tube structures approximately 15–20 nm in diameter and microns in length. Scale bars: 100 nm.

Supporting Information Figure S3a, the **bare-NT** system formed long tubelike structures ~15–20 nm in diameter and often many micrometers in length with both the walls and central pore clearly visible. Incorporating the RGDS epitope yielded identical structures (Figure 2b and Supporting Information Figure S3b), confirming that the peptide did not affect the nanotube formation. We also examined the samples by conventional TEM, which further supported that the **bare-NT** and **RGDS-NT** systems were indistinguishable (Supporting Information Figure S4). On the basis of these investigations, we concluded that splitting s1 into two fragments and attaching the RGDS peptide to s1a does not prevent or perturb the self-assembly of the nanotubes or noticeably decrease their length. Indeed, by looking at Figure 1c it is clear that the peptide is a minor component of the final construct and thus unlikely to present a steric or electrostatic obstacle to the DNA assembly. This ability to control the nanostructure independently of the biological signal is a great advantage of this system and is a challenging task for many alternative peptide only based assemblies, where the epitope is often of comparable or greater size than the self-assembling motif.

We next investigated whether the RGDS epitope was displayed on the surface of the tubes and therefore available for cell signaling. To investigate the availability of the peptide

epitope, we monitored the adhesion of 3T3 fibroblasts on surfaces coated with the DNA tubes. We chose this cell line as a test system due to its well-characterized response to the RGDS peptide, with cells displaying a dramatic increase in attachment and spreading on RGDS-modified surfaces.<sup>36</sup> We modified positively charged surfaces consisting of (3-aminopropyl)-triethoxysilane (APTES) coated glass surfaces with the negatively charged **bare-NT** or **RGDS-NT** and allowed the tubes to adhere overnight. Following removal of unbound DNA, fibroblasts were plated on the DNA-coated surfaces; as a control we used DNA-free APTES-modified glass (which we term **APTES-glass**). After attachment and spreading, the cells were stained to visualize their actin network and allow comparison of their areas. The number of cells and the average cell area were determined using image analysis (see Supporting Information for details). As shown in Figure 3, the fibroblasts

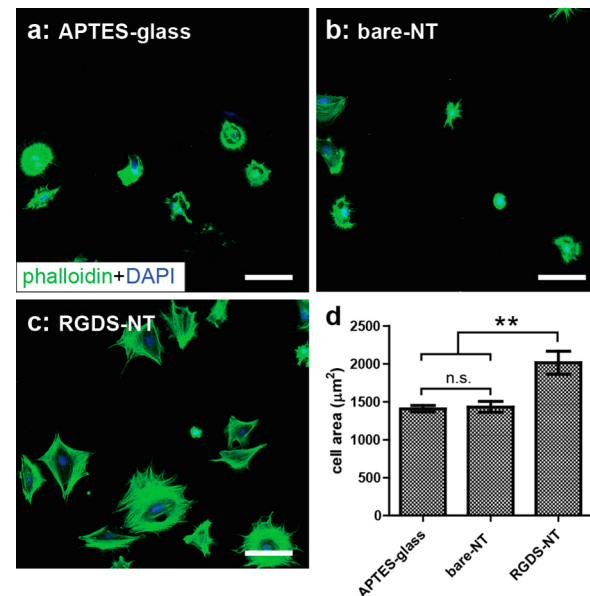


**Figure 3.** Fibroblast adhesion and spreading on DNA nanotube surfaces. Fibroblast cells were seeded on glass slides coated with APTES (a), or APTES slides coated with the unmodified DNA nanotubes (b), or the RGDS-modified nanotubes (c). Following a 3 h incubation, the cell area was determined using image analysis. (d) Graph of cell area, demonstrating the significantly larger size of the fibroblasts cultured on the RGDS-NT coated surfaces. Scale bars: 100  $\mu\text{m}$ . ( $n = 3$ , \*\*  $p < 0.01$ ).

adhered readily on all three substrates. However, cells on the **RGDS-NT**-coated surface spread more and acquired a polygonal shape, accompanied by bundling of actin filaments. Quantification of the projected cell area demonstrated ~40% increase in the average cell area on the **RGDS-NT** coating over the **APTES-glass** and **bare-NT**-coated surfaces ( $2013 \pm 151 \mu\text{m}^2$  versus  $1408 \pm 42 \mu\text{m}^2$  and  $1431 \pm 72 \mu\text{m}^2$ , respectively, Figure 3d). This observation suggests the RGDS epitopes are displayed on the exterior of the nanotube surface because if they were located inside the tube, we would expect **RGDS-NT** and **bare-NT** to behave similarly given the identical morphology of the tubes.

In order to characterize the DNA coatings on the APTES-modified glass, we generated fluorescent nanotubes by incorporating strand s3 with a 3' fluorescein dye, as previously reported.<sup>31</sup> We generated fluorescent versions of **bare-NT** and

RGDS-NT and adsorbed them on APTES-modified surfaces according to the same procedure as for the nonfluorescent systems. Following rinsing, we imaged the surfaces using confocal microscopy to visualize the surface morphology that the cells would be exposed to upon plating. As can be seen in Figure 4a,b (and Supporting Information Figure S5a,b), both

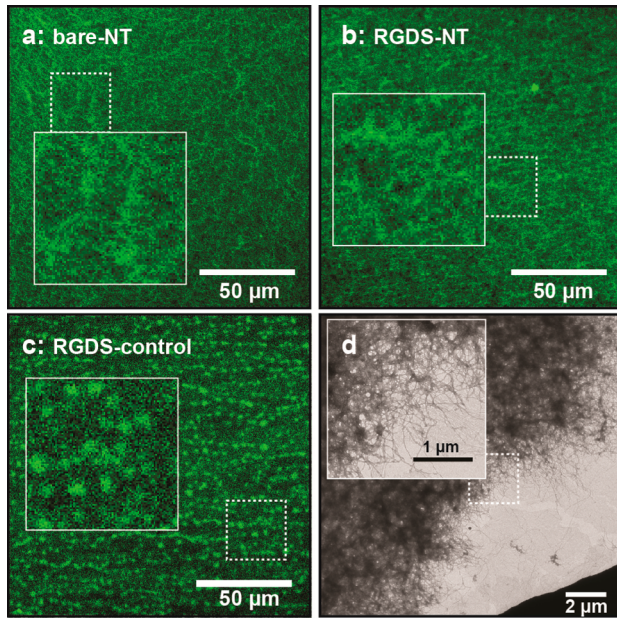


**Figure 4.** Morphology of DNA nanotube surfaces. Fluorescent DNA samples for the **bare-NT** (a), **RGDS-NT** (b), or **RGDS-control** (c) systems were coated on APTES-modified slides and imaged using confocal microscopy. The systems that formed nanotubes (a and b) showed a dense coating of fibrous material on the surface, whereas the **RGDS-control** (c, which cannot form tubes) showed amorphous aggregates on the surface. (d) Conventional TEM images of the **RGDS-NT** system often show dense mats of fibers, similar to what is seen with the fluorescent images. The **bare-NT** sample looks indistinguishable from the **RGDS-NT** sample by TEM (see Supporting Information). Insets show a magnified picture of the area in the dotted box.

**bare-NT** and **RGDS-NT** show a dense, tangled network of fluorescent fiber-like material on the surface. At this resolution, it is impossible to determine the fine structure of these networks, but their fibrous nature suggests the presence of bundled, one-dimensional structures on the surface. This morphology parallels the dense network of fibers sometimes seen by conventional TEM (Figure 4d). Furthermore, the thickness of the DNA coating was measured to be  $\sim 1 \mu\text{m}$  (from the confocal vertical stack), indicating that it consists of many layers of entangled nanotubes.

One of the advantages of DNA-based scaffolds, as mentioned above, is that the nanostructure can be controlled independently of the biological functionality. To demonstrate this property, we constructed a “structural control” system where we included s1a-RGDS, s1b, and s2–4 but omitted strand s5 from the annealing mixture (Supporting Information Figure S6a). This system (which we term **RGDS-control**) prevented the formation of tiles and did not yield any nanotubes by TEM, though occasionally aggregated structures were observed (Supporting Information Figure S6b,c). We highlight that **RGDS-control** has an equal concentration of RGDS epitope and an almost equal amount of total DNA compared with

**RGDS-NT** system but lacks well-defined nanostructures. Indeed, coating fluorescently labeled **RGDS-control** on the APTES-modified glass surface yielded a dramatically different morphology compared with **RGDS-NT** or **bare-NT** with globular and uneven DNA aggregates visible on the surface (Figure 4c and Supporting Information Figure S5c), similar to the aggregated structures occasionally seen by TEM.

Having demonstrated that we can incorporate bioactive peptides into these DNA-based nanotubes and that we can control the nanoscale morphologies obtained, we examined whether these functional nanostructures could be used as substrates to promote the survival and differentiation of neural stem cells (NSCs) into neurons. The development of biomaterials for the selective differentiation of stem cells in order to replace cells lost to injury or disease is a challenging task. One particularly attractive target is neural stem cells, as they self-renew and are committed to the neural lineage, effectively differentiating into neurons, astrocytes, and oligodendrocytes. This target is of great interest in regenerative medicine because new neurons are needed for therapies of neurodegenerative diseases such as Parkinson’s and Alzheimer’s, therapies for traumatic brain injury, and radiation-induced damage of neurons, prevalent especially in pediatric patients of brain tumors. In many injury models, NSCs that are generally quiescent are activated and differentiate into glial scar-forming astrocytes that can inhibit recovery,<sup>37,38</sup> and thus suppression of astrogliosis has been a thoroughly investigated strategy for biomaterials-based treatments for spinal cord injury.<sup>39,40</sup> In addition, NSCs, which have been shown to provide trophic factors favorable to neural recovery, can serve as an expandable cell population for implantation into the injured or diseased nervous system.<sup>41</sup> Biomaterials that can maintain stem cell state or bias NSCs differentiation toward neurons and away from astrocytes can thus serve as promising scaffolds for cell injection and therapy.

The RGDS epitope displayed on the DNA nanotubes is a ligand for  $\beta 1$ -integrin, a laminin receptor highly expressed on NSCs that regulates their adhesion, survival, and proliferation in response to cues from the ECM.<sup>42–44</sup> It was recently suggested that higher levels of  $\beta 1$ -integrin in NSCs correlate with increased self-renewal capacity, and that  $\beta 1$ -integrin signaling may play a role in limiting the generation of astrocytes from NSCs in vitro.<sup>45,46</sup> Furthermore, our previous work found that peptide amphiphile nanofibers bearing the IKVAV epitope derived from laminin, an ECM protein found in the nervous system and a ligand for  $\beta 1$ -integrin, were extremely potent for the selective differentiation of NSCs into neurons, with a concomitant suppression of astrocyte development.<sup>24</sup> We therefore tested the RGDS-modified nanotubes for their ability to promote NSC adhesion, suppress their differentiation into astrocytes, and enhance their differentiation into neurons.

We isolated NSCs from the subventricular zone (SVZ) of postnatal day 1 mice and plated them in differentiation media on the different DNA or DNA-peptide coatings. After allowing the cells to adhere for 2 h, we removed unbound NSCs and cultured the remaining cells for 7 days on the surfaces. Following this time period, the cells were fixed and expression of MAP2 (to visualize neurons) or GFAP (to visualize astrocytes) was quantified using immunocytochemistry. We point out that in these experiments, the final cell mixture is usually heterogeneous, and aside from neurons and astrocytes there is a fraction of undifferentiated cells and other cell types not distinguished by the antibodies used.

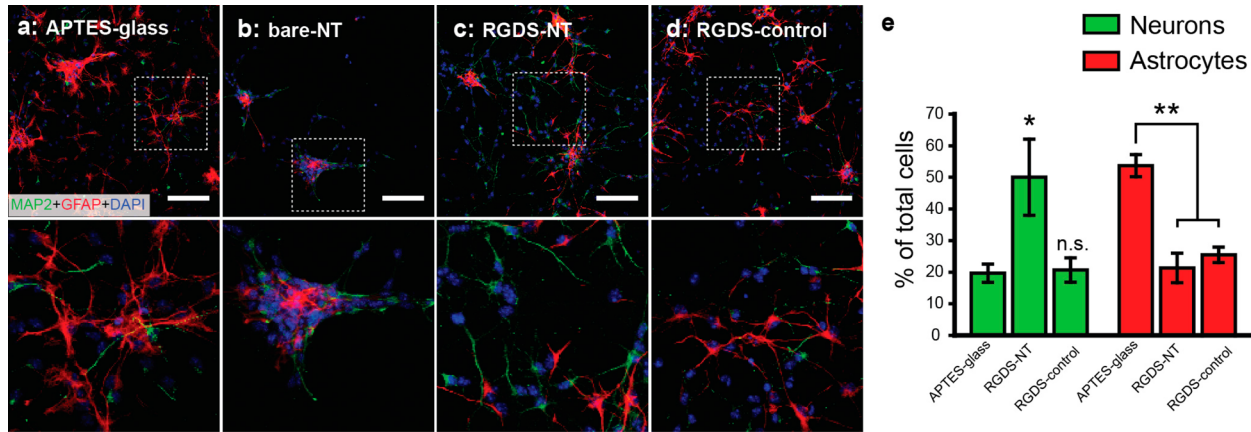


**Figure 5.** Differentiation of neural stem cells on DNA nanotube substrates. (a–d) Confocal microscopy images of NSCs after 7 days of culture on the surfaces indicated. MAP2 (green) indicates neurons, GFAP (red) indicates astrocytes, and DAPI (blue) stains the nuclei. (e) Quantification of the fraction of cells that differentiate into a given lineage ( $n = 3$ , \*  $p < 0.05$ , \*\*  $p < 0.01$ ). Scale bars: 100  $\mu\text{m}$ .

NSCs have a strong tendency to aggregate with one another in culture unless they encounter a highly favorable substrate, so we first investigated whether our surfaces coated with DNA nanotubes provided a good environment for the cells to adhere. The uncoated **APTES-glass** surfaces proved to be a good substrate for NSC adhesion with cells well-distributed and bound to the surface and minimal cell clumping (Figure 5a and Supporting Information Figure S8a), indicating a preference of the cells for the substrate rather than one another. By contrast, NSCs plated on **bare-NT** coated slides showed very poor adhesion with the majority of cells clumping together into ill-defined aggregates indicative of cells adhering to one another rather than to the substrate (Figure 5b and Supporting Information Figures S9a, S10). In great contrast, surfaces covered with **RGDS-NT** provided a good substrate for NSC adhesion with well-distributed cells and minimal clumping (Figure 5c Supporting Information Figure S8b). To confirm that this outcome was not due to a nonspecific effect of the peptide, we plated the NSCs on DNA nanotubes modified with the nonbioactive mutated control peptide **RGES**.<sup>47</sup> The synthesis and purification of the s1a-RGES conjugate, and the nanotube formation (**RGES-NT**) were identical to that of the **RGDS-NT** system (see Supporting Information). Unlike the **RGDS-NT** system, however, the **RGES-NT** surfaces were very poor substrates, and did not support NSC adhesion or differentiation. The cells either clumped together in similar fashion to those on the **bare-NT** surfaces or failed to show differentiation into any of the lineages tested (Supporting Information Figure S9b). Also, the **RGDS-control** system, which contains an equal amount of peptide as **RGDS-NT** but lacks tubelike architecture, supported cell adhesion as well (Figure 5d), suggesting that the aggregated DNA coatings shown in Figure 4c do present enough RGDS signal to help cells attach to the surface. These results suggest that the RGDS epitope is indeed responsible for NSC adhesion to the surfaces.

Next, we examined whether the various substrates had a different effect on NSC differentiation. For this purpose, we quantified the relative fractions of neurons and astrocytes in the three systems that showed good cell adhesion: **APTES-glass**, **RGDS-NT**, and **RGDS-control**. In order to investigate the effect of the substrates on NSC differentiation, we only considered cells that were well-dispersed on the surface. Several reports have controlled the relative cell–cell communication and shown its effect on stem cell fate,<sup>48–50</sup> but this potentially

confounding variable was beyond the scope of this study. The **bare-NT** and **RGES-NT** samples showed cells almost exclusively in aggregates, so we did not quantify the relative fractions of neurons and astrocytes for these surfaces. As can be seen in Figure 5a, a large fraction of NSCs cultured on **APTES-glass** differentiated into astrocytes that often had a well-spread type 1 morphology, similar to activated astrocytes following injury.<sup>51–53</sup> These results were in line with previous observations that stiff substrates like glass tend to bias NSC differentiation toward astrocytes.<sup>54,55</sup> Interestingly, we found that the **RGDS-NT** substrate appeared to yield a higher percentage of neurons than **APTES-glass**, and the astrocytes generated tend to have a more type 2 morphology (less proliferative and bearing long processes).<sup>52,53</sup> Indeed, cell type quantification (Figure 5e) revealed a 2.5-fold increase in the fraction of neurons on the **RGDS-NT** sample compared with **APTES-glass** ( $50.0 \pm 12.0\%$  versus  $19.7 \pm 2.9\%$ ) and a very significant reduction in the fraction of astrocytes ( $21.3 \pm 4.7\%$  versus  $53.7 \pm 3.5\%$ ). The **RGDS-control** sample, lacking nanotube architecture, yielded a similar decrease in the astrocyte fraction ( $25.7 \pm 2.4\%$  versus  $53.7 \pm 3.5\%$ ) relative to the **APTES-glass**, but effectively no change in the fraction of neurons developed ( $20.7 \pm 3.8\%$  versus  $19.7 \pm 2.9\%$ ), suggesting that both the epitope and the nanoscale morphology might be playing distinct roles in the differentiation process.

Our results support the role of the RGDS epitope in suppressing NSC differentiation into astrocytes, as both **RGDS-NT** and **RGDS-control** have a significantly lower proportion of astrocytes compared with **APTES-glass**. However, the fact that **RGDS-NT** yielded a much higher fraction of neurons compared with the **RGDS-control** systems suggests that the nanotube morphology is playing a distinct role in promoting neurogenesis. The RGDS activates  $\beta 1$ -integrin, which is known to promote maintenance of a stem-like state,<sup>44,45</sup> so it is possible that in the **RGDS-control** system a larger fraction of cells remain undifferentiated, whereas the tube morphology in **RGDS-NT** induces differentiation to neurons. To investigate this possibility, we carried out a set of experiments to determine the fraction of cells that express nestin (a neural stem cell marker) in each of the three systems. Indeed, we found a trend toward increased nestin expression in **RGDS-control** compared with **RGDS-NT** or **APTES-glass** (Supporting Information Figure S11).

We hypothesized that more than one factor might be responsible for the large increase in neural differentiation on RGDS-NT substrates relative to **RGDS-control**. The nanotube morphology itself may be directly responsible for the selective differentiation of the NSCs to neurons, with cells sensing the underlying morphology at the nanometer scale. A number of reports have showed the ability of the substrate to bias differentiation of neural stem cells into neurons. For example, culturing NSCs on aligned micropatterned substrates resulted in nearly twice as many neurons as astrocytes.<sup>56</sup> In addition, culturing NSCs on electrospun fibers resulted in greater neuronal differentiation when the fibers had a ~700 nm diameter.<sup>57</sup> These examples, however, use components with feature sizes much larger than the DNA-peptide nanotubes, and although NSCs have been shown to adhere and differentiate on carbon nanotube coatings (which have diameters closer to the RGDS-NT system),<sup>58</sup> no selective effect of the substrate was probed. The mechanical properties of the underlying DNA substrates could also contribute to the difference in cell fate, as stiffness has been shown to play a central role in NSC differentiation, with softer substrates greatly promoting neural differentiation and suppressing astrogliosis.<sup>54,55</sup> The thick layer of intertwined nanotubes in RGDS-NT may present a softer substrate to the NSCs, thus biasing them more toward neurons.

One final factor that could result in the difference between the RGDS-NT and RGDS-control systems is the distance between peptide epitopes. A number of studies have shown that the nanoscale spacing and relative disorder of RGD ligands play critical roles in mesenchymal stem cell adhesion and differentiation.<sup>59–62</sup> The RGDS-NTs display the peptide with a regular spacing of 14 nm in one direction, and 4 nm in the other (Figure 1), which is well below the 70 nm threshold for effective integrin signaling. The RGDS-ctrl samples, on the other hand, likely display the RGDS signal in a much less predictable or repetitive manner, especially given the heterogeneous nature of the aggregates seen in Figure 4c. It should be noted that previous studies have focused on mesenchymal stem cells, so it is unclear if this trend translates to the NSCs investigated here, but this subject is an interesting area for future work.

We have demonstrated the use of a co-assembled bioactive DNA/peptide-DNA supramolecular nanostructure that promotes biological adhesion and subsequent differentiation of neural stem cells into neurons and not astrocytes. This system revealed that both the nanotube architecture and the epitope were critical to achieve this dramatic selectivity. In addition to this architectural control, future possibilities with these hybrid systems may include the spatial<sup>12,63,64</sup> and dynamic<sup>65</sup> control of multiple signal display. The integration of peptides in DNA nanotechnology thus offers many exciting opportunities to expand the field of regenerative medicine.

## ■ ASSOCIATED CONTENT

### Supporting Information

Synthesis, purification, and characterization details for all peptides and peptide-DNA conjugates, details of cell culture, imaging, and quantification, additional TEM images (both cryogenic and conventional) of all systems described, additional fluorescent surface characterization images, additional neuron and astrocyte images, and nestin staining results. This material is available free of charge via the Internet at <http://pubs.acs.org>.

## ■ AUTHOR INFORMATION

### Corresponding Author

\*E-mail: s-stupp@northwestern.edu.

### Present Address

(S.S.) Department of Biology, Clarkson University, 8 Clarkson Avenue, Potsdam, New York 13699, United States.

### Author Contributions

The manuscript was written through contributions of all authors. All authors have given approval to the final version of the manuscript.

### Notes

The authors declare no competing financial interest.

## ■ ACKNOWLEDGMENTS

This project was supported by the Biomaterials Research Partnerships, funded by the National Institutes of Health/National Institute of Biomedical Imaging And Bioengineering Award No. SRO1EB003806-09. N.S. acknowledges support from the IIN Postdoctoral Fellowship and the Northwestern International Institute for Nanotechnology, and from a NIH Ruth L. Kirschstein NRSA postdoctoral fellowship under Award No. 1F32NS077728-01A1. R.F. acknowledges support from an EMBO Long-Term Postdoctoral Fellowship (ALTF 233-2012). H.A.N. acknowledges support from the Craig H. Neilsen Foundation postdoctoral grant. F.T. acknowledges support from the Royal Thai Government. We acknowledge the following Northwestern University facilities: Simpson Querrey Institute for BioNanotechnology (SQI) Peptide Core, the SQI Equipment Core, Electron Probe Instrumentation Center (EPIC), the Northwestern University Biological Imaging Facility (BIF) (generously supported by the NU Office for Research), and the Northwestern University Cell Imaging Facility and a Cancer Center Support Grant (NCI CA060553).

## ■ REFERENCES

- (1) Seeman, N. C. *Chem. Biol.* **2003**, *10*, 1151–1159.
- (2) Wilner, O. I.; Willner, I. *Chem. Rev.* **2012**, *112*, 2528–2556.
- (3) Rothemund, P. W. K.; Ekani-Nkodo, A.; Papadakis, N.; Kumar, A.; Fygenson, D. K.; Winfree, E. *J. Am. Chem. Soc.* **2004**, *126*, 16344–16352.
- (4) Yan, H.; Park, S. H.; Finkelstein, G.; Reif, J. H.; LaBean, T. H. *Science* **2003**, *301*, 1882–1884.
- (5) Lo, P. K.; Karam, P.; Aldaye, F. A.; McLaughlin, C. K.; Hamblin, G. D.; Cosa, G.; Sleiman, H. F. *Nat. Chem.* **2010**, *2*, 319–328.
- (6) Winfree, E.; Liu, F. R.; Wenzler, L. A.; Seeman, N. C. *Nature* **1998**, *394*, 539–544.
- (7) Zheng, J.; Birktoft, J. J.; Chen, Y.; Wang, T.; Sha, R.; Constantinou, P. E.; Ginell, S. L.; Mao, C.; Seeman, N. C. *Nature* **2009**, *461*, 74–77.
- (8) Rothemund, P. W. K. *Nature* **2006**, *440*, 297–302.
- (9) Douglas, S. M.; Dietz, H.; Liedl, T.; Hoegberg, B.; Graf, F.; Shih, W. M. *Nature* **2009**, *459*, 414–418.
- (10) Sacca, B.; Niemeyer, C. M. *Angew. Chem. Int. Ed.* **2012**, *51*, 58–66.
- (11) Pinheiro, A. V.; Han, D.; Shih, W. M.; Yan, H. *Nat. Nanotechnol.* **2011**, *6*, 763–772.
- (12) Sacca, B.; Niemeyer, C. M. *Chem. Soc. Rev.* **2011**, *40*, 5910–5921.
- (13) Ke, Y.; Lindsay, S.; Chang, Y.; Liu, Y.; Yan, H. *Science* **2008**, *319*, 180–183.
- (14) Douglas, S. M.; Bachelet, I.; Church, G. M. *Science* **2012**, *335*, 831–834.
- (15) Lee, H.; Lytton-Jean, A. K. R.; Chen, Y.; Love, K. T.; Park, A. I.; Karagiannis, E. D.; Sehgal, A.; Querbes, W.; Zurenko, C. S.; Jayaraman,

- M.; Peng, C. G.; Charisse, K.; Borodovsky, A.; Manoharan, M.; Donahoe, J. S.; Truelove, J.; Nahrendorf, M.; Langer, R.; Anderson, D. G. *Nat. Nanotechnol.* **2012**, *7*, 389–393.
- (16) Liu, X.; Xu, Y.; Yu, T.; Clifford, C.; Liu, Y.; Yan, H.; Chang, Y. *Nano Lett.* **2012**, *12*, 4254–4259.
- (17) Liu, X.; Liu, Y.; Yan, H. *Isr. J. Chem.* **2013**, *53*, 555–566.
- (18) Wang, F.; Lu, C.-H.; Willner, I. *Chem. Rev.* **2014**, *114*, 2881–2941.
- (19) Aldaye, F. A.; Senapati, W. T.; Silver, P. A.; Way, J. C. *J. Am. Chem. Soc.* **2010**, *132*, 14727–14729.
- (20) Um, S. H.; Lee, J. B.; Park, N.; Kwon, S. Y.; Umbach, C. C.; Luo, D. *Nat. Mater.* **2006**, *5*, 797–801.
- (21) Xing, Y.; Cheng, E.; Yang, Y.; Chen, P.; Zhang, T.; Sun, Y.; Yang, Z.; Liu, D. *Adv. Mater.* **2011**, *23*, 1117–1121.
- (22) Stephanopoulos, N.; Ortony, J. H.; Stupp, S. I. *Acta Mater.* **2013**, *61*, 912–930.
- (23) Hartgerink, J. D.; Beniash, E.; Stupp, S. I. *Science* **2001**, *294*, 1684–1688.
- (24) Silva, G. A.; Czeisler, C.; Niece, K. L.; Beniash, E.; Harrington, D. A.; Kessler, J. A.; Stupp, S. I. *Science* **2004**, *303*, 1352–1355.
- (25) Chow, L. W.; Bitton, R.; Webber, M. J.; Carvajal, D.; Shull, K. R.; Sharma, A. K.; Stupp, S. I. *Biomaterials* **2011**, *32*, 1574–1582.
- (26) Webber, M. J.; Tongers, J.; Newcomb, C. J.; Marquardt, K.-T.; Bauersachs, J.; Losordo, D. W.; Stupp, S. I. *Proc. Natl. Acad. Sci. U.S.A.* **2011**, *108*, 13438–13443.
- (27) Lee, S. S.; Huang, B. J.; Kaltz, S. R.; Sur, S.; Newcomb, C. J.; Stock, S. R.; Shah, R. N.; Stupp, S. I. *Biomaterials* **2013**, *34*, 452–459.
- (28) Mata, A.; Geng, Y.; Henrikson, K. J.; Aparicio, C.; Stock, S. R.; Satcher, R. L.; Stupp, S. I. *Biomaterials* **2010**, *31*, 6004–6012.
- (29) Shah, R. N.; Shah, N. A.; Lim, M. M. D. R.; Hsieh, C.; Nuber, G.; Stupp, S. I. *Proc. Natl. Acad. Sci. U.S.A.* **2010**, *107*, 3293–3298.
- (30) O'Neill, P.; Rothmund, P. W. K.; Kumar, A.; Fygenson, D. K. *Nano Lett.* **2006**, *6*, 1379–1383.
- (31) O'Neill, P. R.; Young, K.; Schiffels, D.; Fygenson, D. K. *Nano Lett.* **2012**, *12*, 5464–5469.
- (32) Hersel, U.; Dahmen, C.; Kessler, H. *Biomaterials* **2003**, *24*, 4385–4415.
- (33) Webber, M. J.; Tongers, J.; Renault, M.-A.; Roncalli, J. G.; Losordo, D. W.; Stupp, S. I. *Acta Biomater.* **2010**, *6*, 3–11.
- (34) Agard, N. J.; Baskin, J. M.; Prescher, J. A.; Lo, A.; Bertozzi, C. R. *ACS Chem. Biol.* **2006**, *1*, 644–648.
- (35) Debets, M. F.; van Berkel, S. S.; Schoffelen, S.; Rutjes, F. P. J. T.; van Hest, J. C. M.; van Delft, F. L. *Chem. Commun.* **2010**, *46*, 97–99.
- (36) Massia, S. P.; Hubbell, J. A. *J. Cell Biol.* **1991**, *114*, 1089–1100.
- (37) Barnabe-Heider, F.; Goritz, C.; Sabelstrom, H.; Takebayashi, H.; Pfrieger, F. W.; Meletis, K.; Frisen, J. *Cell Stem Cell* **2010**, *7*, 470–482.
- (38) Gao, X.; Chen, J. *Exp. Neurol.* **2013**, *239*, 38–48.
- (39) Tysseling-Mattiace, V. M.; Sahni, V.; Niece, K. L.; Birch, D.; Czeisler, C.; Fehlings, M. G.; Stupp, S. I.; Kessler, J. A. *J. Neurosci.* **2008**, *28*, 3814–3823.
- (40) Weightman, A. P.; Pickard, M. R.; Yang, Y.; Chari, D. M. *Biomaterials* **2014**, *35*, 3756–3765.
- (41) Sabelstrom, H.; Stenudd, M.; Reu, P.; Dias, D. O.; Elfineh, M.; Zdunek, S.; Damberg, P.; Goritz, C.; Frisen, J. *Science* **2013**, *342*, 637–640.
- (42) Kazanis, I.; Ffrench-Constant, C. *Dev. Neurobiol.* **2011**, *71*, 1006–1017.
- (43) McGraw, J.; Hiebert, G. W.; Steeves, J. D. *J. Neurosci. Res.* **2001**, *63*, 109–115.
- (44) Campos, L. S.; Leone, D. P.; Relvas, J. B.; Brakebusch, C.; Fassler, R.; Suter, U.; fFrench-Constant, C. *Development* **2004**, *131*, 3433–3444.
- (45) Leone, D. P.; Relvas, J. B.; Campos, L. S.; Hemmi, S.; Brakebusch, C.; Fassler, R.; fFrench-Constant, C.; Suter, U. *J. Cell Sci.* **2005**, *118*, 2589–2599.
- (46) Pan, L.; North, H. A.; Sahni, V.; Jeong, S. J.; McGuire, T. L.; Berns, E. J.; Stupp, S. I.; Kessler, J. A. *PLoS One* **2014**, *9*, e104335.
- (47) Sur, S.; Matson, J. B.; Webber, M. J.; Newcomb, C. J.; Stupp, S. I. *ACS Nano* **2012**, *6*, 10776–10785.
- (48) Tang, J.; Peng, R.; Ding, J. *Biomaterials* **2010**, *31*, 2470–2476.
- (49) Peng, R.; Yao, X.; Cao, B.; Tang, J.; Ding, J. *Biomaterials* **2012**, *33*, 6008–6019.
- (50) Yao, X.; Peng, R.; Ding, J. *Adv. Mater.* **2013**, *25*, 5257–5286.
- (51) Sun, D.; Jakobs, T. C. *Neuroscientist* **2012**, *18*, 567–588.
- (52) Raff, M. C.; Miller, R. H.; Noble, M. *Nature* **1983**, *303*, 390–396.
- (53) Sensenbrenner, M.; Lucas, M.; Deloulme, J. C. *J. Mol. Med.* **1997**, *75*, 653–663.
- (54) Saha, K.; Keung, A. J.; Irwin, E. F.; Li, Y.; Little, L.; Schaffer, D. V.; Healy, K. E. *Biophys. J.* **2008**, *95*, 4426–4438.
- (55) Sur, S.; Newcomb, C. J.; Webber, M. J.; Stupp, S. I. *Biomaterials* **2013**, *34*, 4749–4757.
- (56) Recknor, J. B.; Sakaguchi, D. S.; Mallapragada, S. K. *Biomaterials* **2006**, *27*, 4098–4108.
- (57) Christopherson, G. T.; Song, H.; Mao, H.-Q. *Biomaterials* **2009**, *30*, 556–564.
- (58) Jan, E.; Kotov, N. A. *Nano Lett.* **2007**, *7*, 1123–1128.
- (59) Graeter, S. V.; Huang, J.; Perschmann, N.; Lopez-Garcia, M.; Kessler, H.; Ding, J.; Spatz, J. P. *Nano Lett.* **2007**, *7*, 1413–1418.
- (60) Huang, J.; Grater, S. V.; Corbellini, F.; Rinck, S.; Bock, E.; Kemkemer, R.; Kessler, H.; Ding, J.; Spatz, J. P. *Nano Lett.* **2009**, *9*, 1111–1116.
- (61) Wang, X.; Ye, K.; Li, Z.; Yan, C.; Ding, J. *Organogenesis* **2013**, *9*, 280–286.
- (62) Wang, X.; Yan, C.; Ye, K.; He, Y.; Li, Z.; Ding, J. *Biomaterials* **2013**, *34*, 2865–2874.
- (63) Pedersen, R. O.; Loboa, E. G.; LaBean, T. H. *Biomacromolecules* **2013**, *14*, 4157–4160.
- (64) Shaw, A.; Lundin, V.; Petrova, E.; Fordos, F.; Benson, E.; Al-Amin, A.; Herland, A.; Blokzijl, A.; Hogberg, B.; Teixeira, A. I. *Nat. Methods* **2014**, *11*, 841–846.
- (65) Zhang, D. Y.; Seelig, G. *Nat. Chem.* **2011**, *3*, 103–113.